

**On the possibility of
convective overturning
in the Słupsk Furrow
overflow of the Baltic Sea***

doi:10.5697/oc.53-2.771
OCEANOLOGIA, 53 (3), 2011.
pp. 771–791.

© Copyright by
Polish Academy of Sciences,
Institute of Oceanology,
2011.

KEYWORDS

Baltic Sea
Dense water overflows
Gravity currents
Convective
overturns

VICTOR ZHURBAS^{1,2}
JÜRI ELKEN²
VADIM PAKA³
JAN PIECHURA^{4,*}
IRINA CHUBARENKO³
GERMO VÄLI²
NIKOLAY GOLENKO³
SERGEY SHCHUKA¹

¹ P. P. Shirshov Institute of Oceanology,
Russian Academy of Sciences,
Nakhimovsky Prospect 36, Moscow 117997, Russia

² Marine Systems Institute,
Tallinn University of Technology,
Akadeemia tee 21, Tallinn 12118, Estonia

³ Atlantic Branch of the P. P. Shirshov Institute of Oceanology,
Russian Academy of Sciences,
Prospect Mira 1, Kaliningrad 236000, Russia

⁴ Institute of Oceanology,
Polish Academy of Sciences,
Powstańców Warszawy 55, Sopot 81–712, Poland;
e-mail: piechura@iopan.gda.pl

*corresponding author

Received 29 April 2011, revised 11 July 2011, accepted 2 August 2011.

* The work was sponsored by the Russian Foundation for Basic Research (grant No. 09-05-00479) and the Estonian Science Foundation (grant No. 7328).

The complete text of the paper is available at <http://www.iopan.gda.pl/oceanologia/>

Abstract

Closely spaced CTD transects across the Słupsk Furrow displayed a ‘downward-bending’ of salinity contours below the salinity interface on the southern flank due to a transverse circulation in the saline water overflow. Numerical simulation of a gravity current in an idealized channel with geometry, dimensions and initial density stratification all much the same as in the Słupsk Furrow was applied to verify whether the downward-bending could be transformed into an inverted density stratification. Some arguments in favour of the possibility of convective overturning due to the differential transverse advection beneath the gravity current, brought on by the numerical simulations, are discussed.

1. Introduction

Channelized gravity currents play a key role in the deep water exchange between ocean basins and the formation of deep water masses (Baringer & Price 1997, Mauritzen et al. 2005, Peters et al. 2005). Well-known examples of channelized gravity flows are the Mediterranean outflow (Johnson et al. 1994, Baringer & Price 1997), the Faroe Bank Channel overflow in the North Atlantic (Borenäs & Lundberg 1988, Johnson & Sanford 1992), the Vema Channel overflow in the South Atlantic (Hogg & Zenk 1997) and the Red Sea outflow (Peters et al. 2005).

The Coriolis force will be important for channelized gravity currents when the Rossby number of these flows (defined as $Ro = |U/Wf|$, where U is the mean downstream velocity, W is the channel width, and f is the Coriolis parameter) is less than order 1 (Cossu et al. 2010). When $Ro \ll 1$, the flow is substantially slower than a non-rotating flow with the same density contrast. Because of the Earth’s rotation, the transverse density structure of channelized gravity flows becomes asymmetrical. The density interface goes down to the left of the down-channel flow (in the Northern Hemisphere) in accordance with geostrophic balance. There is a pronounced spreading (pinching) of the pycnocline on the right-hand (left-hand) flank, so that the interface looks wedge-shaped (e.g. Petré & Walin 1976, Borenäs & Lundberg 1988, Johnson & Sanford 1992). The pool of the densest water often lies on the left-hand flank (Paka 1996, Paka et al. 1998) and the downward bending of near-bottom isopycnals appears on the right-hand flank. Moreover, some observations demonstrate an ultimate bending with isopycnals becoming nearly vertical, so that the vertical homogeneity and pure horizontal density gradient are established on the right-hand flank, while the left-hand flank remains essentially free of horizontal density variations (Umlauf & Arneborg 2009a, Umlauf et al. 2010).

In accordance with a theory by Wåhlin (2002, 2004), the topographic downward steering of the frictionally controlled gravity current along a channel implies that the transverse Ekman transport in the bottom boundary layer (BBL) is balanced by the transverse geostrophic transport due to the down-channel tilt of the interface. Umlauf & Arneborg (2009b) and Umlauf et al. (2010) showed that the nearly geostrophically balanced interfacial jet plays a key role, transporting interfacial fluid to the right of the down-channel flow. Since the interfacial jet is directed to the right of the down-channel flow, the net transverse transport in the deeper layer – the sum of the Ekman transport and the geostrophic constituent – is directed to the left of the down-channel flow to balance the interfacial jet transport. Note that the features of the secondary circulation in channelized gravity currents and the related asymmetry of transverse density structure can be explained, apart from the interfacial jet and the Ekman and geostrophic transport in BBL, by the rotating hydraulic theory (e.g. Hogg 1983).

As a result of the secondary transverse circulation, less dense water moves down along the sloping bottom on the right-hand flank, and the resulting down-bending of density contours is potentially transformed into inverted density stratification. Therefore, it cannot be ruled out that the convective overturning caused by differential advection plays some role in the formation of vertically homogeneous BBL with pure horizontal density gradients on the right-hand flank (Volker Mohrholz, Lars Umlauf, and Lars Arneborg, personal communication). Convectively-driven mixing in the BBL over a sloping bottom caused by the secondary circulation was reported by Moum et al. (2004), who observed parcels of fluid adjacent to the bottom that were less dense relative to the fluid immediately above displaying an inverted vertical gradient of potential density of about $6.0 \times 10^{-5} \text{ kg m}^{-4}$.

The objective of this paper is to explore the possibility of convective overturning as applied to the Słupsk Furrow overflow in the Baltic Sea, based on field data and numerical simulations.

2. Data

The geographical focus of our study is the Słupsk Furrow (SF), a channel-like topographic constriction in the southern Baltic Sea between the Bornholm Basin and the Eastern Gotland/Gdańsk basins (Figure 1). It is approximately 90 km long, 30–32 km wide (as estimated by the distance between 50-m isobaths) and 63–92 m deep in the deepest passage. The western part of the Furrow next to the Słupsk Sill has a descending slope of about 5×10^{-4} , while the eastern part of the Furrow is characterized by

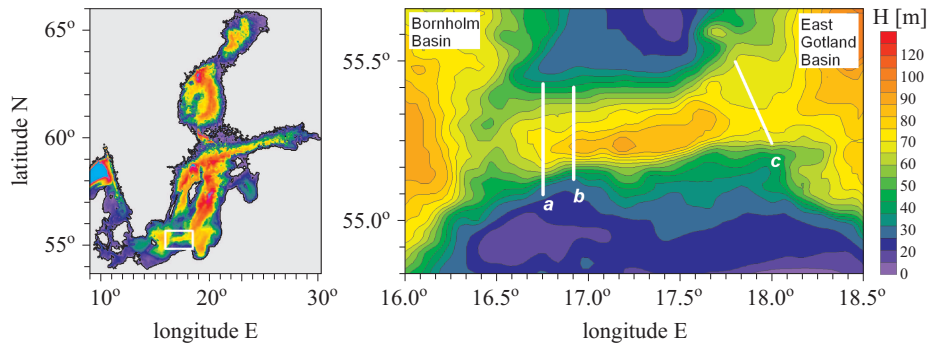


Figure 1. Bathymetric map of the Baltic Sea (left) and a close-up of the Słupsk Furrow (right). The white lines, labelled *a*, *b* and *c*, depict the transects across the Furrow with the closely spaced CTD measurements presented in Figure 2

a bottom rising in the direction of the eastward overflow. The Furrow is the only pathway for saline water of North Sea origin to enter the deep basins of the Baltic Proper and ventilate them laterally.

Because of the relatively small dimensions of the Baltic Sea (1600 km long, 200 km wide on average and 55 m deep), transient weather patterns with a time scale of a few days superimpose significant perturbations in deep water transport due to compensation flows (e.g. Krauss & Brüggge 1991). Gravity current transport in the Słupsk Furrow was recently calculated by Borenäs et al. (2007) using the rotating hydraulic theory. The transverse structure of the Słupsk Furrow overflow has been examined by Paka (1996), Paka et al. (1998, 2006) and Piechura & Beszczyńska-Möller (2003).

To get detailed patterns of the transverse density structure of the Słupsk Furrow overflow, data from closely spaced CTD profiles with a horizontal resolution of 200–500 m, approaching the bottom as close as 1–2 m, were addressed. Such a detailed CTD profiling was made possible as a result of a winch-operated tow-yo technique at a speed of 5 knots (Paka 1996). Such a technique is widely used during the Baltic cruises of the Polish and Russian research vessels (e.g. Piechura & Beszczyńska-Möller 2003, Paka et al. 2006). A typical time scale required to complete a CTD transect across SF is 3 hours, so the transects can be considered synoptic.

Figure 2 presents salinity versus distance and depth measured on three transects across the Słupsk Furrow. Since the temperature variation makes only a minor contribution to the density variability in the Baltic halocline (within a few percent of that of salinity), the salinity contours almost coincide with the potential density contours. The salinity patterns of Figure 2a, b were measured in the western part of SF, where the channel slopes down in the downstream (i.e. eastward) direction at an angle of approx. 5×10^{-4}

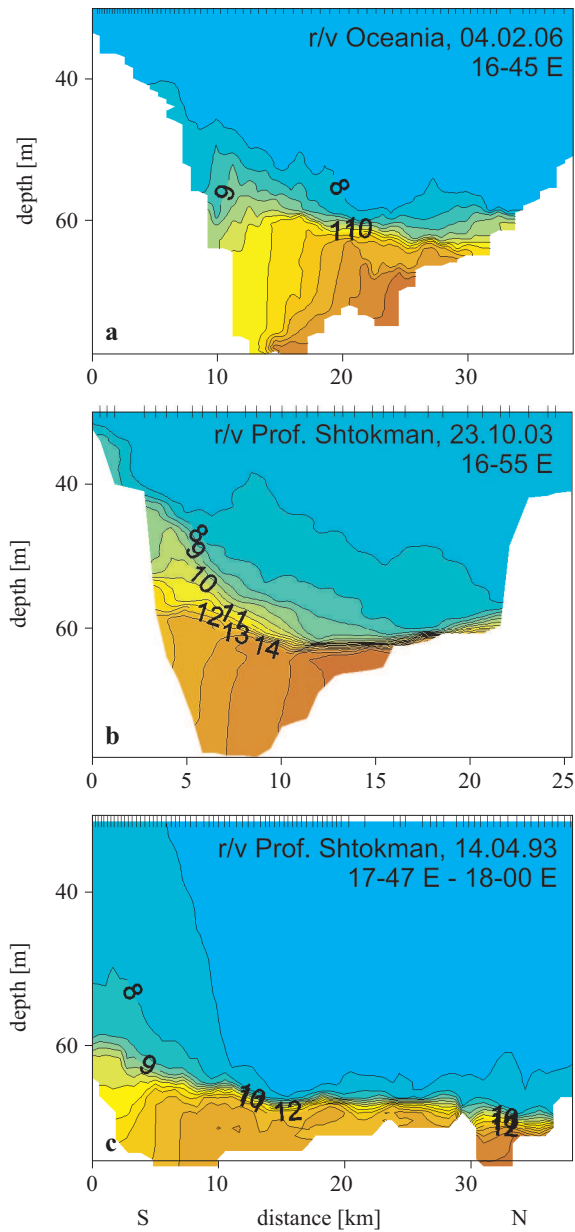


Figure 2. Salinity versus distance and depth measured on three transects across the Słupsk Furrow. In this and the next figures the salinity units are PSU. The positions of the three transects are shown in Figure 1. The panels show the name of the research vessel, the date of measurements and the longitude of the transects. The vertical dashes at the top of the panels show where the vertical profiles were made

radians, while Figure 2c shows the transverse salinity structure at the eastern exit of SF (for the location of the transects, see Figure 1).

A striking feature, common to all three salinity cross-sections, is the well-pronounced effect of the downward-bending of near-bottom isohalines and, therefore, isopycnals on the right-hand (southern) flank of the eastward gravity current. The near-bottom salinity contours fall nearly vertically, so that there is a vertically homogeneous bottom boundary layer (BBL) with almost pure lateral gradients of salinity/density. One could suggest that such a vertically homogeneous layer was formed by the coupled effect of differential advection due to the secondary circulation in the gravity flow and vertical mixing. Nonetheless, there remains a doubt about the very nature of the vertical mixing: has it been caused by shear flow instability, convective overturning, or both?

The only signature of convective overturning which can be obtained from vertical profiles is the inversion of potential density (salinity) in the bottom layer. Some of the vertical profiles did show weak density inversions in the vertically quasi-homogeneous bottom layer of SF (with the density difference and the thickness of the inverted layer of about $3 \times 10^{-3} \text{ kg m}^{-3}$ and several metres respectively), but such inversions are not reliable in view of the magnitude of possible instrumental errors. To obtain some arguments in favour of the possibility of convective overturning caused by the secondary circulation in the SF gravity current, the numerical experiment described below was carried out.

3. Simulation

The simulation experiment was performed mainly using the Princeton Ocean Model – POM (Blumberg & Mellor 1987). POM is a free surface, hydrostatic, sigma coordinate hydrodynamic model with an imbedded second and a half moment turbulence closure sub-model (Mellor & Yamada 1982). For comparison, the simulation experiment was repeated with a z -coordinate version of POM and MIKE 3, a 3D modelling system for free surface flows (www.mikebydhi.com). MIKE 3 is a commercial software package developed and supported by the Danish Hydraulic Institute (DHI). MIKE 3 has hydrostatic and non-hydrostatic options, and we applied the former in order to make a straightforward comparison with POM. The substantial difference between POM and MIKE 3 in our case is that the latter is used in a z -level formulation with either the Smagorinsky subgrid scale model turbulent closure (Smagorinsky 1963) for both vertical and lateral mixing or a second moment k - ε turbulence closure for vertical mixing.

The Słupsk Furrow overflow is expected to depend strongly on the existing irregularities of bottom topography, which can bias the flow performance and complicate the interpretation of the numerical simulation results on the transverse secondary circulation. For this reason it seemed worth starting with the numerical simulations of a channelized gravity current in an idealized sloping channel, the size, geometry and initial salinity stratification of which are comparable to those of the Słupsk Furrow (Figure 3). For the sake of clarity, the x axis of the channel is directed eastwards, like the Słupsk Furrow. The channel is 300 km long, 40 km wide, and 150 m deep; its cross-section is parabolic in shape. The channel consists of 3 parts, each 100 km long, and only the central part has a slope of 5×10^{-4} . The channel is closed at $x = 0$ and $x = 300$ km. The finite difference grid cell size is $2/3$ km in the x and y directions. Vertically there are 63 sigma layers in POM and 75 equal z -layers in MIKE 3, so that both models provide an identical vertical resolution in the mid cross-section of the channel (63 sigma or z layers being no more than 2 m thick). To achieve a more detailed vertical resolution of possible density inversions in BBL under the gravity current, the final runs of the sigma coordinate POM and the z -coordinate POM were performed with 129 sigma layers and 150 z -layers, so that the vertical grid size did not exceed 1 m. The temperature distribution in an initially motionless channel was taken to be uniform at $T = 5^\circ\text{C}$; the initial salinity field is shown in Figure 3. Heat and salt fluxes across the sea surface and bottom are absent, as is wind forcing; bottom friction is controlled by the roughness parameter (0.01 m). Note that the simulation of ocean overflows using an idealized topography of the model domain has been undertaken by several researchers. For instance, Ezer (2006) used an idealized topography of the Faroe Bank

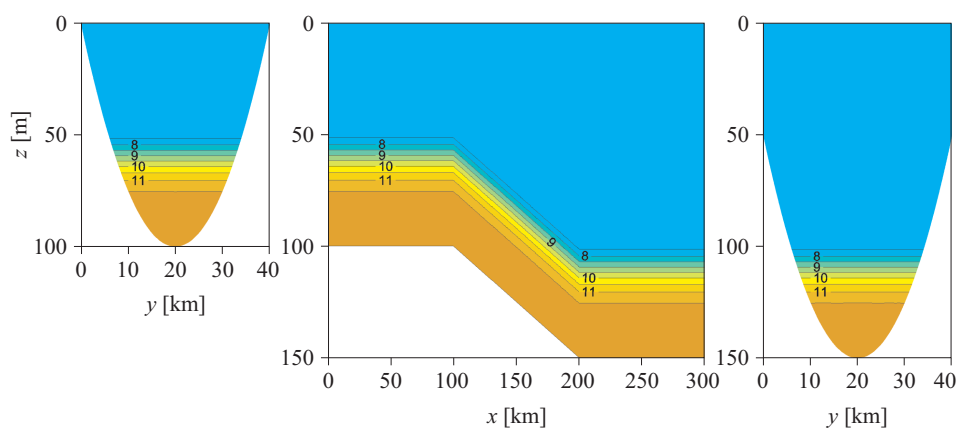


Figure 3. Geometry of an idealized channel and the initial salinity distribution

Channel (FBC) to simulate the FBC Overflow, and Umlauf et al. (2010) performed 2D numerical experiments in an infinitely long and deep channel with an idealized cross-section of parabolic shape and a constant down-channel tilt to simulate the bottom gravity current of saline water of North Sea origin passing through a small, 10 m deep and 10 km wide, channel-like constriction north of the Kriegers Shoal in the Arkona Basin, (western Baltic Sea) (Umlauf & Arneborg 2009a).

The maximum velocity of shallow water internal waves is $c_{\max} = (BH)^{1/2}$, where B and H are respectively the bulk buoyancy and thickness of the lower layer (see equation (1) below). For the artificial channel shown in Figure 3 c_{\max} is estimated at $c_{\max} = 1.1 \text{ m s}^{-1}$, so that the time scale t_{wave} for the disturbances (shallow water waves) generated at the boundaries to reach the mid section is $t_{\text{wave}} = 150 \text{ km}/1.1 \text{ m s}^{-1} \approx 1.6$ days. In fact, the numerical simulations showed that strong wave-like disturbances appeared in front of the downstream boundary 4 days after the simulation onset and reached the mid-section in 2 extra days. For this reason the analysis that follows will be restricted to a time limit of 6 days.

Figure 4 presents the distributions of salinity as well as along-channel and cross-channel velocities in the mid cross-section of the channel obtained by POM after 2 and 4 days from the start of the simulation. The dense saline water flows down the channel with a velocity U of about 0.4 m s^{-1} , so the formation of a gravity current is clearly seen. The interface between the saline water involved in the gravity current and the overlying fresher water slopes down to the north, entirely in accordance with geostrophic equilibration in the y (i.e. cross-channel) direction. The highest speeds are observed right below the interface, and there is a continuous decrease of the along-channel velocity towards the bottom.

The cross-channel salinity/density structure displays, apart from the interface tilt caused by the geostrophic adjustment of the underlying gravity current, a well-pronounced asymmetry consisting of the pinching and spreading of the interfacial isohalines/isopycnals on the left- and right-hand sides of the gravity current (looking downstream) and a displacement of the pool of densest water to the left-hand side (i.e. to the north in our case). Moreover, the salinity contours below the interface become vertical in the southern and central parts, displaying the presence of considerable horizontal salinity/density gradients along with the vanishingly small vertical gradients. In the northern part such horizontal salinity/density gradients are absent. Note that the simulated features of the transverse salinity/density structure (Figure 4) show reasonable quantitative correspondence with the observations (Figure 2): both the observations and simulations display a vertically quasi-homogeneous BBL about 20 m thick

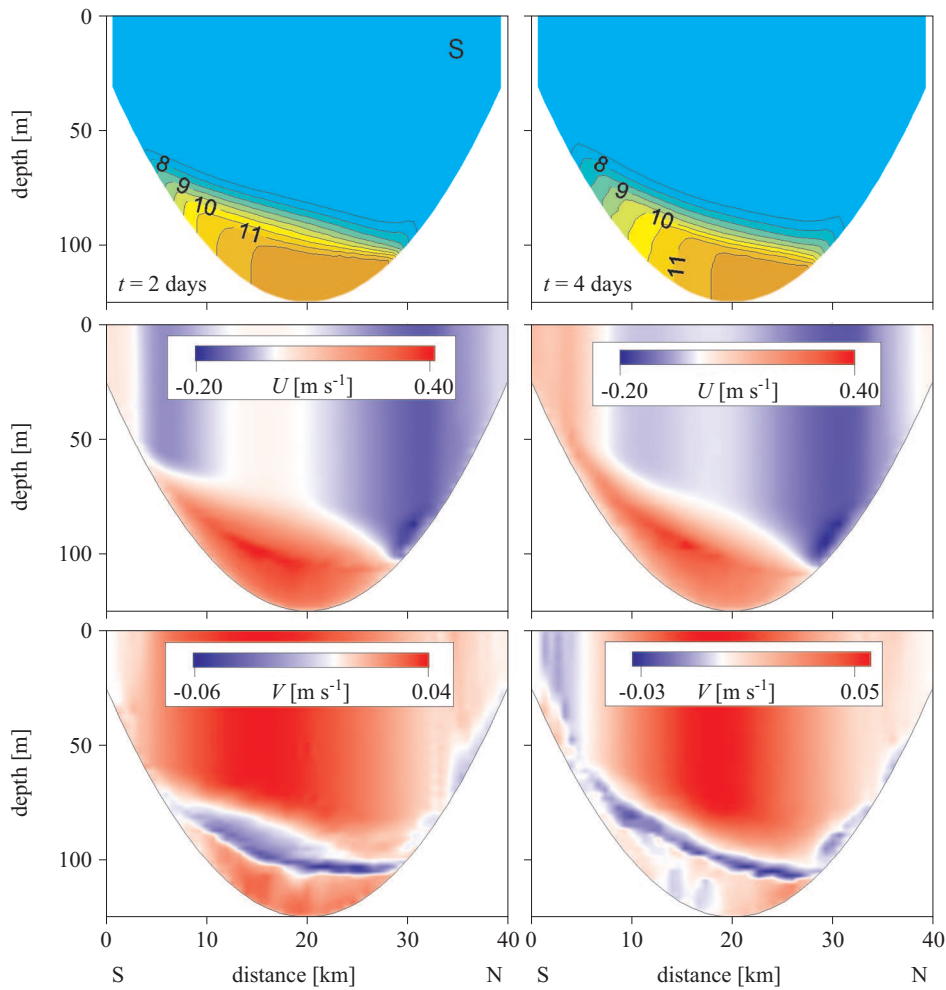


Figure 4. Salinity (top), along-channel velocity (middle) and cross-channel velocity (bottom) in the mid cross-section at $t = 2$ and 4 days simulated with POM

with a horizontal salinity gradient of about 0.2 PSU km^{-1} in the centre and the right-hand flank of the gravity flow.

The evolution of a transverse circulation in the course of the formation of a channelized rotating gravity current is illustrated in the bottom panels of Figure 4. The formation is accompanied by a clockwise (looking downstream) transverse circulation caused by the geostrophically balanced interfacial jet (Umlauf & Arneborg 2009b), and the sum of the Ekman transport and the opposite geostrophic transport below the interface. Being mostly positive (northward) below the core of the gravity current and negative (southward) in the interface just above the core, transverse

velocities do not exceed 0.06 m s^{-1} at $t = 2$ days. The transverse circulation modifies the salinity/density field, producing a downward-bending of density contours and horizontal density gradients in BBL on the southern flank of the channel which, in accordance with the thermal wind relation, can provide a geostrophically balanced decrease of the gravity current velocity towards the bottom without the Ekman veering; such a process is referred to as Ekman layer arrest (Garrett et al. 1993). As a result, the northward (positive) transverse velocities summing the Ekman velocities and the geostrophic velocities due to the down-channel pressure gradient fade below the core and even become slightly negative, while the southward transverse jet-like flow with speeds of about 0.03 m s^{-1} still persists in the density interface just above the core (see the bottom right-hand plot in Figure 4). Such a reversal of the near-bottom transverse current is caused by the thermal wind shear due to the presence of lateral, cross-channel density gradients below the interface (Umlauf & Arneborg 2009b, Umlauf et al. 2010).

All the above-mentioned features of the channelized gravity current revealed by means of simulation, including the pinching-spreading effect, the existence of a lateral density gradient and vertical density homogenization in the southern flank below the core of the current, the establishment of a transverse circulation with a southward transverse interfacial jet and a near-bottom current reversal, have been observed in a channel-like constriction of the Arkona Basin (Umlauf & Arneborg 2009a) and reproduced numerically by Burchard et al. (2009).

To check whether a rotating gravity current is frictionally controlled, one has to estimate different terms of the bulk (vertically integrated) down-channel momentum balance and the non-dimensional Froude and Ekman numbers characterizing the variety of flow regimes. Following e.g. Arneborg et al. (2007), the bulk buoyancy B and thickness H of a gravity current may be defined as

$$BH = \int_{z_b}^{\infty} b \, dz, \tag{1}$$

$$\frac{1}{2}BH^2 = \int_{z_b}^{\infty} b(z - z_b)dz,$$

where $b = -g(\rho - \rho_{\infty})/\rho_{\infty}$ is the negative buoyancy of gravity flow with respect to the overlying ambient fluid of density ρ_{∞} and zero buoyancy ($b \rightarrow 0$ at $z \rightarrow \infty$), $g = 9.81 \text{ m s}^{-2}$ is the acceleration due to gravity, and the lower integration limit lies at the bottom ($z = z_b$). The Froude number (Fr), the Ekman number (Ek) and the Ekman layer depth are introduced as

$$\text{Fr} = \frac{U}{(-BH)^{1/2}}, \quad \text{Ek} = \left(\frac{\delta_E}{H}\right)^2, \quad \delta_E = \frac{u_*^2}{fU}, \quad (2)$$

where U is the vertically averaged (bulk) velocity of the gravity current, $u_*^2 = -\tau_x/\rho_\infty$ is the squared friction velocity, τ_x is the down-channel bottom stress and f is the Coriolis parameter.

The bulk down-channel baroclinic and barotropic pressure gradient forces $-BC_x$ and BT_x respectively – as well as the Coriolis force CO_x acting on the gravity current can be estimated as

$$BC_x = \int_{z_b}^{\infty} \left(\int_{z_b}^z \frac{\partial b}{\partial x} dz \right) dz, \quad BT_x = -fv_0(z_i - z_b), \quad CO_x = \int_{z_b}^{z_i} fv dz, \quad (3)$$

where v_0 is the y -component of the geostrophic velocity at the sea surface, v is the y -component of the flow velocity, $z = z_i$ corresponds to the upper boundary of the layer of dense water defined as the level where salinity is 7.2 PSU (i.e. a little bit above 7 PSU, the undisturbed value of the upper layer salinity).

Time series of the above-defined constituents of down-channel momentum budget calculated for the central point of the mid cross-section of the channel using the POM simulation (Figure 5, top panel) show that within a period of 1–4 days the bottom friction force $-u_*^2$ is balanced by the sum of the pressure gradient force and the Coriolis force $BC_x + BT_x + CO_x$, while after 4 days the bottom friction force gradually disappears and eventually the negative value of $BC_x + BT_x$ balances the positive value of CO_x . Formally such a balance does not fit the ‘classical’ bulk down-channel momentum budget in a frictionally controlled gravity current when the pressure gradient force due to the down-channel tilt of the interface balances the bottom friction (assuming that the interfacial entrainment stress is negligible) while the pressure gradient force due to the cross-channel tilt of the interface is geostrophically balanced by the gravity flow velocity (Wählín 2002). However, one may suggest that for the closed channel geometry shown in Figure 3 the gravity current in the mid cross-section is skewed, so that the down- and cross-channel tilt of the interface may differ from that of the down- and cross-stream. Based on this suggestion, one may perform a standard transformation from the down-channel-oriented Cartesian co-ordinates xy to the downstream-oriented ones $x'y'$ using the constraint $CO_{x'} = 0$, where x' is the downstream axis, and formulate the downstream momentum budget instead of the down-channel one.

Time series of the downstream constituents of the bulk momentum budget $BC_{x'} + BT_{x'}$, $-u_*'^2$ and the angle φ between the $x'y'$ and xy coordinate systems (Figure 5, bottom panel) clearly show after an initial 1 day period the balance between the positive $BC_{x'} + BT_{x'}$ and the negative

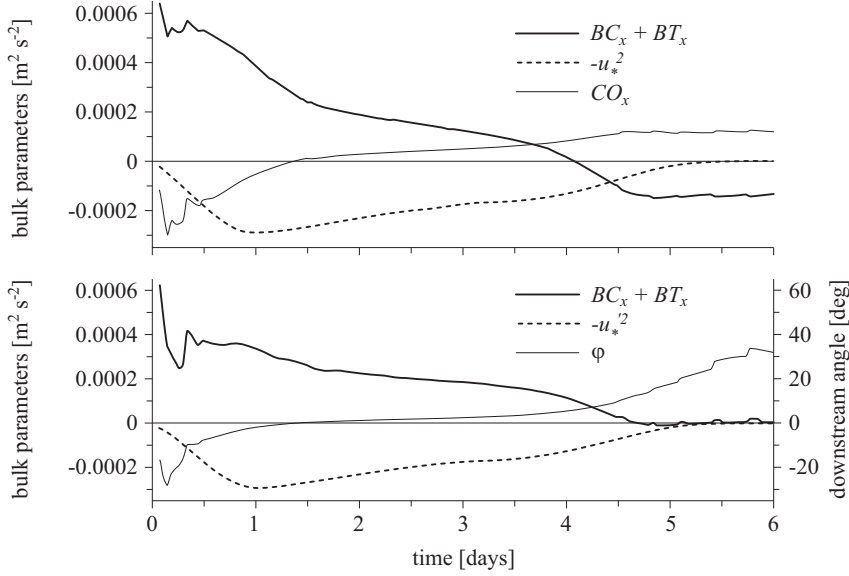


Figure 5. Time series of the down-channel (top) and down-stream (bottom) bulk momentum budget constituents of the gravity current as well as the downstream angle φ , calculated for the central point of the mid cross-section of the channel using the POM simulation

$-u_*'^2$, so that the gravity current can be undoubtedly treated as frictionally controlled. Note that $BC_{x'} + BT_{x'}$ and $-u_*'^2$ disappear simultaneously with time, while the absolute values of the baroclinic and barotropic downstream pressure gradient constituents, $BC_{x'}$ and $BT_{x'}$, remain large (not shown). In any case, after 5 days the gravity current no longer exists (see Figure 5, the bottom panel). Note that the downstream angle is negative ($-20^\circ > \varphi > -2^\circ$) at $t < 1$ day (before the gravity current is formed), slowly increases from $\varphi \approx -2^\circ$ to $\varphi \approx 5^\circ$ within the period of 1 day $< t < 4$ days when there is a frictionally controlled gravity current, and increases faster to $\varphi \approx 17^\circ$ at $t = 5$ days when the bottom stress vanishes.

The mean values of the Froude number, the Ekman number and the Ekman depth, averaged over the period of 1–4 days, were estimated at $Fr = 0.27$, $Ek = (u_*'^2 U^{-1} f^{-1} H^{-1})^2 = 2.7 \times 10^{-2}$ and $\delta_E = u_*'^2 U^{-1} f^{-1} = 5.8$ m. In accordance with laboratory experiments by Cenedese et al. (2004), such values of Fr and Ek correspond to a sub-critical ($Fr < 1$) gravity flow of the eddy ($Ek < 0.1$) regime. However, the laboratory experiments were done with a plane slope bottom, so the criterion obtained for the eddy regime ($Ek < 0.1$) cannot be applied to the channelized gravity current unless the channel width is large relative to the gravity current width R . If the gravity current is frictionally controlled, its width is expressed as

$R = \delta_E/S_{x'}$, where $S_{x'}$ is the downstream slope of the interface (Darelius & Wåhlin 2007), which in our case can be obtained from the formula $S_{x'} = (BT_{x'} + BC_{x'})/(B \times H)$. Taking the average for the period of 1–4 days ($BT_{x'} + BC_{x'} = 2 \times 10^{-4} \text{ m}^2 \text{ s}^{-2}$, $B = 0.034 \text{ m}^2 \text{ s}^{-1}$, $H = 35.0 \text{ m}$), we obtain $S_{x'} = 1.7 \times 10^{-4}$ and $R = 50 \text{ km}$. Since the channel width at the undisturbed level of the interface is $\approx 25 \text{ km}$ (see Figure 3), the channel is narrow relative to the potential width of the gravity current, therefore the criterion $\text{Ek} = (u_*'^2 U^{-1} f^{-1} H^{-1})^2 < 0.1$ does not work – the simulation does not display eddy formation. On the other hand, $U f \approx 2.5 \text{ km}$ should be much smaller than the channel width (25 km) in order to develop an asymmetry in a channelized gravity current (Cossu et al. 2010).

In addition to equation (2) there are other definitions of the Ekman depth in turbulent flows, e.g. $\delta_E = 0.4u_*/f$ (Cushman-Roisin 1994, Perlin et al. 2007). This expression is more likely to correspond to the thickness affected by frictional effects (Umlauf & Arneborg 2009a) and yields substantially larger values for the Ekman depth than the expression $\delta_E = u_*'^2/(fU)$ based on the momentum budget. The Ekman depth $\delta_E = u_*/f$, averaged over the simulation period of 1–4 days, is estimated at 47 m, which exceeds the dense layer/gravity current thickness ($H = 34 \text{ m}$) confirming the frictional control of the current.

If entrainment to the gravity current is ignored (this is justified by the balance of $BC_{x'} + BT_{x'}$ and $u_*'^2$ shown in Figure 5), the average speed of a geostrophically balanced, transverse interfacial jet is $v_{\text{mean}} = BS_{x'}/2f$ (Umlauf & Arneborg 2009b). The latter expression can be used to check whether the simulated jet is geostrophically balanced. The bulk buoyancy and the downstream interfacial slope are estimated as $B = 0.035$ and 0.033 m s^{-2} and $S_{x'} = 1.9 \times 10^{-4}$ and 1.0×10^{-4} for the respective moments in time of 2 and 4 days, so the estimates of the mean speed of the jet by the above formula are $v_{\text{mean}} = 0.027$ and 0.014 m s^{-1} . The mean values of the jet speed calculated from analytical expression $v_{\text{mean}} = BS_{x'}/2f$ were found to be twice as small as the simulated maximum values (cf. Figure 4), which is quite reasonable.

Even though the transverse structure of the modelled gravity current in the Słupsk Furrow is found to be similar to that of the Arkona Basin (Arneborg et al. 2007, Umlauf & Arneborg 2009a, Umlauf et al. 2010), these two flows have quite different dimensional and non-dimensional dynamic parameters. The Słupsk Furrow gravity current has a larger width W (25 km vs. 10 km) and thickness H (34 m vs. 11 m) and a smaller mean downstream interfacial slope $S_{x'}$ (1.5×10^{-4} vs. 5.0×10^{-4}), bulk buoyancy B (0.034 m s^{-2} vs. 0.07 m s^{-2}), friction velocity u_* (0.015 m s^{-1} vs. 0.02 m s^{-1}), bulk flow velocity U (0.3 m s^{-1} vs. 0.5 m s^{-1}), Froude number

Fr (0.27 vs. 0.54) and Ekman number $\text{Ek} = (u_*^2 U^{-1} f^{-1} H^{-1})^2$ (2.7×10^{-2} vs. ≈ 1). Though $\text{Ek} \ll 1$ in the case of Ślupsk Furrow, both gravity currents can be regarded as frictionally controlled, because the Ekman depth $\delta_E = 0.4u_*/f$ exceeds H (Umlauf & Arneborg 2009a). That is why in both cases the transverse structure of the gravity current is characterized by the presence of a thin interfacial jet directed to the right of the down-channel flow. Note that in the case when the Ekman layer thickness is much smaller than the channelized gravity flow itself, the transverse velocity structure does not display a thin interfacial jet but a secondary flow field consisting of frictionally induced Ekman transports across the channel in the benthic and interfacial boundary layers and a return flow in the interior (Cossu et al. 2010).

The small value of the Froude number in the Ślupsk Furrow gravity current relative to that of the Arkona Basin ($\text{Fr} = 0.27$ vs. $\text{Fr} = 0.54$) implies a reduced amount of entrainment in the former case. To estimate the entrainment of surrounding waters to a gravity current, one can use a new empirical parameterization suggested by Cenedese & Adduce (2010) based on laboratory and field measurements

$$E = \frac{\text{Min} + A \text{Fr}^\alpha}{1 + A C_{\text{inf}}(\text{FR} + \text{FR}_0)^\alpha}, \quad C_{\text{inf}} = \frac{1}{\text{Max}} + \frac{B}{\text{Re}^\beta}, \quad (4)$$

where $E = w_e/U$ is the entrainment ratio, w_e is the entrainment velocity, $\text{Re} = UH/v$ is the Reynolds number, $v \approx 1.3 \times 10^{-6} \text{ m}^2 \text{ s}^{-1}$ is the kinematic molecular viscosity of water, and $\text{Min} = 4 \times 10^{-5}$, $\text{Max} = 1$, $A = 3.4 \times 10^{-3}$, $\text{Fr}_0 = 0.51$, $\alpha = 7.18$ and $\beta = 0.5$ are empirical constants based on the limited oceanographic and laboratory data available. Substituting the above parameters of gravity flows into equation (4) one obtains $E = 4.03 \times 10^{-5} \approx \text{Min}$ for the simulated gravity flow in the Ślupsk Furrow and $E = 8.0 \times 10^{-5}$ for the Arkona Basin gravity current. Therefore, the entrainment in the Ślupsk Furrow is twice as small as that of the Arkona Basin. Note that the last estimate ($E = 8.0 \times 10^{-5}$) is close to the observed value $E = 6.6 \times 10^{-5}$ (Arneborg et al. 2007).

The simulation of the same flow using MIKE 3 yielded results almost identical to those of POM (cf. Figures 4 and 6). The only difference worth mentioning is an inverted, hydrostatically unstable salinity/density stratification in BBL simulated with MIKE 3 instead of the vertically uniform stratification simulated with POM. This difference can be interpreted as follows. Both models reproduce secondary Ekman flow in BBL directed to the left of the main gravity current, which is able to modify the salinity/density distribution in the channel's cross-section. Being aligned with the sloping seabed, the transverse flow transports less dense water down

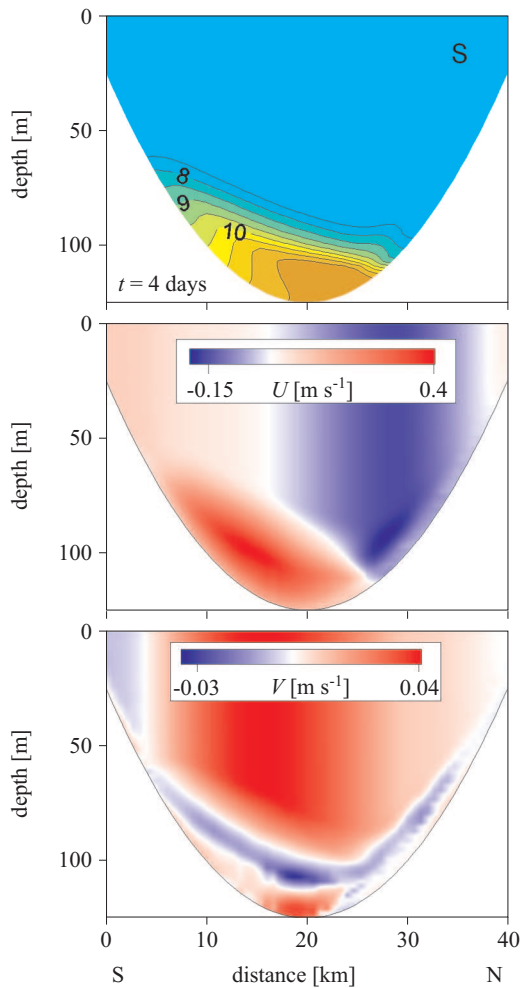


Figure 6. Salinity (top), along-channel velocity (middle) and cross-channel velocity (bottom) in the mid cross-section at $t = 4$ days simulated with MIKE 3 and the Smagorinsky vertical diffusivity

in the southern flank of the channel. Therefore the salinity/density contours bend downwards, displaying a tendency to become vertical and eventually produce inverted, hydrostatically unstable stratification. However, when the density contours approach the vertical, the density stratification weakens and the stratified shear gravity current becomes hydrodynamically unstable, producing turbulent mixing together with vertical homogenization of BBL, thereby establishing a pure horizontal density gradient. This was demonstrated in the POM simulation (Figure 4), where the instability of the stratified shear current is plausibly parameterized by the $2^{1/2}$ moment

turbulence closure (Mellor & Yamada 1982). The parameterization explicitly describes the effect of stratification on vertical mixing, since the vertical turbulent viscosity K_M and heat/salt diffusivity K_H are expressed as

$$\begin{aligned} K_M &= lqS_M(\text{Ri}_t), \\ K_H &= lqS_H(\text{Ri}_t), \end{aligned} \tag{5}$$

where q is the root mean square velocity fluctuation (so that q^2 is the specific kinetic energy of turbulence), l is the external length scale of turbulence, and S_M and S_H are functions of the Richardson number Ri_t

$$\text{Ri}_t = \frac{l^2}{q^2} \frac{g}{\rho_0} \frac{\partial \rho_{pot}}{\partial z}, \tag{6}$$

where ρ_{pot} is the potential density and ρ_0 is the reference density. Note that $\text{Ri}_t < 0$ when stratification is hydrostatically stable (in this case $-(g/\rho_0)(\partial \rho_{pot}/\partial z) \equiv N^2$ is the squared buoyancy frequency), $\text{Ri}_t = 0$ for neutral stratification, and $\text{Ri}_t > 0$ for hydrostatically unstable stratification. For neutral stratification ($\text{Ri}_t = 0$) $S_M = 0.8S_H = 0.39$ and for stable stratification S_M and S_H are infinitesimally small with $|\text{Ri}_t|$ (i.e. $S_M \approx S_H \rightarrow 0$ at $\text{Ri}_t \rightarrow -\infty$, and, for example, $S_M \approx S_H = 0.014$ at $\text{Ri}_t = -1$). And finally, for unstable stratification, S_M and S_H increase rapidly with the growth of an unstable (inverted) potential density gradient, achieving in the POM code a practical limit of $S_M = 0.75S_H = 12.7$ at $\text{Ri}_t = 0.028$ and further retaining the same limiting value at $\text{Ri}_t > 0.028$. Therefore, even when an inverted density gradient was formed as a result of differential transverse advection, the above described drastic increase of vertical eddy diffusivity/viscosity at unstable density stratification would mix up the inversion and establish vertical quasi-homogeneity, so that the residual inverted gradients would be strongly depressed.

Unlike POM, the MIKE 3 simulation is based on the Smagorinsky subgrid scale model turbulent closure, which does not explicitly allow for stratification. The Smagorinsky subgrid diffusivity is simply taken to be proportional to the product of the squared vertical grid size and velocity gradients, implying that the model is able to resolve the instability of shear stratified flow and the related intensification of vertical mixing. However, since we apply a hydrostatic version of MIKE 3 and take a horizontal grid size much larger than the vertical one, the model cannot explicitly reproduce the instabilities of shear stratified flow (e.g. the Kelvin-Helmholtz instability) and, therefore, the apparent vertical diffusivity remains underestimated. As a result, there is no homogenization of the

bottom layer due to vertical mixing and an inverted density stratification forms. Note that the POM simulations shown in Figure 4 frequently display inverted density stratification in BBL under the gravity current, too, but the inverted density jump is small enough (of the order of $10^{-2} \text{ kg m}^{-3}$ or less – too small to be identified visually on salinity/density sections and profiles) for the bottom layer to be considered highly homogeneous.

To reinforce the validation of the inverted density gradients, the above-described numerical experiment with gravity current in an idealized sloping channel was reproduced using three different modelling tools: (a) σ -coordinate and (b) z -coordinate POM with 1 m vertical resolution, and (c) MIKE 3 with a k - ε turbulence closure. If independent models based on different approaches reproduce the same effect (e.g. density inversions), then we believe that confidence in the reality of this effect will increase. All three models were found to produce frequent events of salinity/density inversions in BBL under the gravity current, with the inverted salinity difference within the range of 10^{-4} – 10^{-2} (see Figure 7) and the vertical scale of 1–10 m (not shown here). The inverted salinity difference was computed as the maximum salinity on a simulated vertical profile minus the salinity at the point of the profile closest to the bottom, so that the difference is positive if there is an inversion and zero if there is no inversion. The frequent presence of inverted density gradients implies that the differential advection related to the transverse circulation can produce convective overturning of the bottom boundary layer in a channelized gravity current.

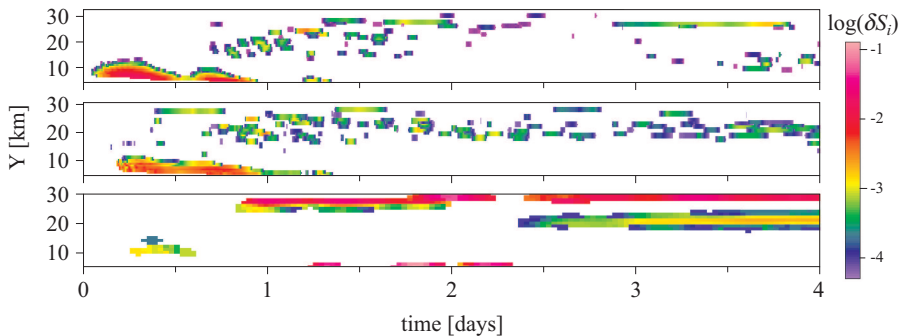


Figure 7. Salinity inversion value in the bottom layer of the mid cross-section δS_i versus distance and time simulated with (top) σ -coordinate and (middle) z -coordinate versions of POM, and (bottom) MIKE 3 equipped with a k - ε turbulence closure. The salinity inversion value is defined as the maximum salinity on a vertical profile minus the salinity at the point of the profile closest to the bottom

4. Summary and conclusions

Closely spaced CTD transects performed across the Słupsk Furrow aboard Polish and Russian research vessels have frequently displayed an asymmetrical pattern of salinity/density in the permanent halocline. A characteristic feature of the pattern is a downward-bending of salinity contours below the salinity interface and the establishing of almost pure lateral gradients on the southern flank of the Furrow. The down-bending is known to be a result of the secondary circulation in a gravity current – the Słupsk Furrow overflow in our case – when there is a transverse current in the bottom boundary layer directed to the left (north) of the gravity current in accordance with Ekman dynamics. Owing to the secondary transverse circulation, less dense water moves down along the sloping bottom on the right-hand flank, and the resulting downward-bending of the density contours is potentially transformed into the inverted density stratification. Numerical simulation of gravity current in an idealized channel with geometry, dimensions and initial density stratification comparable with that of the Słupsk Furrow was applied to verify the possibility of overturning due to the differential transverse advection beneath the gravity current. To increase confidence in the results of these simulations, the above-described numerical experiment was performed using three different modelling tools: (a) σ -coordinate and (b) z -coordinate POM with a 1 m vertical resolution, and (c) MIKE 3 with a k - ε turbulence closure. All three models showed identical features of the channelized gravity current, e.g. the geostrophically balanced transverse jet in the interface layer directed to the right of the gravity current, the down-bending of density contours below the interface and establishing almost pure lateral gradients on the right hand flank, and the presence of frictional control. While the above-mentioned features were known before (e.g. Umlauf et al. 2010), the frequent events of weak density inversions recorded in the BBL beneath the core of the simulated gravity current is a new finding. We believe that such inversions simulated with three different numerical models may be considered an important argument in favour of the possibility of convective overturning events in the Słupsk Furrow overflow. Since the convective overturning in BBL has the potential to considerably increase the intensity of mixing, such events deserve further investigation.

Acknowledgements

We thank the anonymous reviewers for their valuable and stimulating comments.

References

- Arneborg L., Fiekas V., Umlauf L., Burchard H., 2007, *Gravity current dynamics and entrainment – a process study based on observations in the Arkona Basin*, J. Phys. Oceanogr., 37 (8), 2094–2113, doi:10.1175/JPO3110.1.
- Baringer M., Price J.F., 1997, *Mixing and spreading of the Mediterranean outflow*, J. Phys. Oceanogr., 27(8), 1654–1677, doi:10.1175/1520-0485(1997)027<1654:MASOTM>2.0.CO;2.
- Blumberg A.F., Mellor G.L., 1987, *A description of a coastal ocean circulation model*, [in:] *Three dimensional ocean models*, N.S. Heaps (ed.), American Geophys. Union, Washington, D.C., 1–16.
- Borenäs K., Hietala R., Laanearu J., Lundberg P., 2007, *Some estimates of the Baltic deep water transport through the Stolpe trench*, Tellus A, 59 (2), 238–248, doi:10.1111/j.1600-0870.2006.00221.x.
- Borenäs K.M., Lundberg P.A., 1988, *On the deep-water flow through the Faroe Bank Channel*, J. Geophys. Res., 93 (C2), 1281–1292, doi:10.1029/JC093iC02p01281.
- Burchard H., Janssen F., Bolding K., Umlauf L., Rennau H., 2009, *Model simulations of dense bottom currents in the Western Baltic Sea*, Cont. Shelf Res., 29 (1), 205–220, doi:10.1016/j.csr.2007.09.010.
- Cenedese C., Adduce C., 2010, *A new parameterization for entrainment in overflows*, J. Phys. Oceanogr., 40 (8), 1835–1850. doi:10.1175/2010JPO4374.1.
- Cenedese C., Whitehead J. A., Ascarelli T. A., Ohiwa M., 2004, *A dense current flowing down a sloping bottom in a rotating fluid*, J. Phys. Oceanogr., 34 (1), 188–203, doi:10.1175/1520-0485(2004)034<0188:ADCFDA>2.0.CO;2.
- Cossu R., Wells M. G., Wählin A. K., 2010, *Influence of the Coriolis force on the velocity structure of gravity currents in straight submarine channel systems*, J. Geophys. Res., 115, C11016, doi:10.1029/2010JC006208.
- Cushman-Roisin B., 1994, *Introduction to geophysical fluid dynamics*, Prentice-Hall, Upper Saddle River, N. J., 320 pp.
- Darelius E., Wählin A., 2007, *Downward flow of dense water leaning on a submarine ridge*, Deep-Sea Res. Pt. I, 54 (7), 1173–1188, doi:10.1016/j.dsr.2007.04.007.
- Ezer T., 2006, *Topographic influence on overflow dynamics: idealized numerical simulations and the Faroe Bank Channel overflow*, J. Geophys. Res., 111, C02002, doi:10.1029/2005JC003195.
- Garrett C., MacCready P., Rhines P., 1993, *Boundary mixing and arrested Ekman layers: rotating stratified flow near a sloping bottom*, Annu. Rev. Fluid Mech., 25, 291–323, doi:10.1146/annurev.fl.25.010193.001451.
- Hogg N.G., 1983, *Hydraulic control and flow separation in a multi-layered fluid with applications to the Vema Channel*, J. Phys. Oceanogr., 13 (4), 695–708, doi:10.1175/1520-0485(1983)013<0695:HCAFSI>2.0.CO;2.

- Hogg N.G., Zenk W., 1997, *Long-period changes in the bottom water flowing through Vema Channel*, J. Geophys. Res., 102 (C7), 15636–15646, doi:10.1029/97JC00591.
- Johnson G.C., Sanford T.B., 1992, *Secondary circulation in the Faroe Bank channel outflow*, J. Phys. Oceanogr., 22 (8), 927–933, doi:10.1175/1520-0485(1992)022<0927:SCITFB>2.0.CO;2.
- Johnson G.C., Sanford T.B., Baringer M.O., 1994, *Stress on the Mediterranean outflow plume. Part I: Velocity and water property measurements*, J. Phys. Oceanogr., 24 (10), 2072–2083, doi:10.1175/1520-0485(1994)024<2072:SOTMOP>2.0.CO;2.
- Krauss W., Brügge B., 1991, *Wind-produced water exchange between the deep basins of the Baltic Sea*, J. Phys. Oceanogr., 21 (3), 373–394, doi:10.1175/1520-0485(1991)021<0373:WPWEBT>2.0.CO;2.
- Mauritzen C., Price J., Sanford T., Torres D., 2005, *Circulation and mixing in the Faroese channels*, Deep-Sea Res. Pt. I, 52 (6), 883–913, doi:10.1016/j.dsr.2004.11.018.
- Mellor G.L., Yamada T., 1982, *Development of a turbulence closure model for geophysical fluid problems*, Rev. Geophys., 20 (4), 851–875, doi:10.1029/RG020i004p00851.
- Moum J.N., Perlin A., Klymak J.M., Levine M.D., Boyd T., Kosro P.M., 2004, *Convectively-driven mixing in the bottom boundary layer over the continental shelf during downwelling*, J. Phys. Oceanogr., 34 (10), 2189–2202, doi:10.1175/1520-0485(2004)034<2189:CDMITB>2.0.CO;2.
- Paka V., 1996, *Thermohaline structure of the waters over the cross-sections in the Stupsk Channel of the Baltic Sea in spring, 1993*, Oceanology, 36 (2), 188–198.
- Paka V., Golenko N., Korzh A., 2006, *Distinctive features of water exchange across the Stupsk Sill (a full-scale experiment)*, Oceanologia, 48 (S), 37–54.
- Paka V., Zhurbas V., Golenko N., Stefantsev L., 1998, *Effect of the Ekman transport on the overflow of saline waters through the Stupsk Furrow in the Baltic Sea*, Izv. Atmos. Oceanic Phys., 34 (5), 641–648.
- Perlin A., Moum J.N., Klymak J.M., Levine M.D., Boyd T., Kosro P.M., 2007, *Organization of stratification, turbulence, and veering in bottom Ekman layers*, J. Geophys. Res., 112, C05S90, 12 pp., doi:10.1029/2004JC002641.
- Peters H., Johns W.E., Bower A.S., Fratantoni D.M., 2005, *Mixing and entrainment in the Red Sea outflow plume. Part I: Plume structure*, J. Phys. Oceanogr., 35 (5), 569–583, doi:10.1175/JPO2679.1.
- Petrén O., Walin G., 1976, *Some observations of the deep flow in the Bornholm strait during the period June 1973–December 1974*, Tellus, 28 (1), 74–87, doi:10.1111/j.2153-3490.1976.tb00653.X.
- Piechura J., Beszczyńska-Möller A., 2003, *Inflow waters in the deep regions of the southern Baltic Sea – transport and transformations*, Oceanologia, 45 (4), 593–621.

- Smagorinsky J., 1963, *General circulation experiment with the primitive equations. I. The basic experiment*, Mon. Weather Rev., 91 (3), 99–164, doi:10.1175/1520-0493(1963)091<0099:GCEWTP>2.3.CO;2.
- Umlauf L., Arneborg L., 2009a, *Dynamics of rotating shallow gravity currents passing through a channel. Part I: Observation of transverse structure*, J. Phys. Oceanogr., 39 (10), 2385–2401, doi:10.1175/2009JPO4159.1.
- Umlauf L., Arneborg L., 2009b, *Dynamics of rotating shallow gravity currents passing through a channel. Part II: Analysis*, J. Phys. Oceanogr., 39 (10), 2402–2416, doi:10.1175/2009JPO4164.1.
- Umlauf L., Arneborg L., Hofmeister R., Burchard H., 2010, *Entrainment in shallow rotating gravity currents: a modeling study*, J. Phys. Oceanogr., 40 (8), 1819–1834, doi:10.1175/2010JPO4367.1.
- Wåhlin A.K., 2002, *Topographic steering of dense currents with application to submarine canyons*, Deep-Sea Res. Pt. I, 49 (2), 305–320, doi:10.1016/S0967-0637(01)00058-9.
- Wåhlin A.K., 2004, *Downward channelling of dense water in topographic corrugations*, Deep-Sea Res. Pt. I, 51 (4), 577–590, doi:10.1016/j.dsr.2003.11.002.